PHYSICAL REVIEW B **81**, 020103(R) (2010)

Reorientation of magnetic dipoles at the antiferroelectric-paraelectric phase transition of $Bi_{1-x}Nd_xFeO_3$ ($0.15 \leq x \leq 0.25$)

Igor Levin,[1,*,†,§] Sarah Karimi,[2] Virgil Provenzano,[1] Cindi L. Dennis,[1] Hui Wu,[1] Tim P. Comyn,[3] Tim J. Stevenson,[3] Ronald I. Smith,[4] and Ian M. Reaney[2,*,‡,§]

[1]*National Institute of Standards and Technology, Gaithersburg, Maryland 20899, USA*

[2]*Department of Engineering Materials, University of Sheffield, Sheffield, United Kingdom*

[3]*Institute for Materials Research, University of Leeds, Leeds, United Kingdom*

[4]*ISIS Facility, Rutherford Appleton Laboratory, Didcot, United Kingdom*

(Received 6 November 2009; revised manuscript received 15 December 2009; published 27 January 2010)

Ceramic $Bi_{1-x}Nd_xFeO_3$ solid solutions in the approximate compositional range $0.15 \leq x \leq 0.25$ undergo first-order antiferroelectric (AFE) $\leftrightarrow$ paraelectric (PE) phase transitions between 300 °C and room temperature. The orthorhombic AFE (*Pnam*, $\sqrt{2}a_c \times 2\sqrt{2}a_c \times 4a_c$, where $a_c \approx 4$ Å and is the lattice parameter of an ideal cubic perovskite) and PE (*Pbnm*, $\sqrt{2}a_c \times \sqrt{2}a_c \times 2a_c$) structures differ not only in the type of octahedral tilt system but also in the pattern of *A*-cation (Bi/Nd) displacements. The AFE $\leftrightarrow$ PE transition is accompanied by a large ($\approx$2%) discontinuous volume change similar to that observed at the ferroelectric (FE) $\leftrightarrow$ PE transition in $BiFeO_3$. For all compositions, the structural transition occurs within the *G*-type antiferromagnetic (AFM) state. Variable-temperature magnetic measurements reveal a strong coupling between the AFE $\leftrightarrow$ PE transition and the magnetic ordering. Rietveld refinements using neutron powder-diffraction data demonstrate that the structural transition is accompanied by reorientation of magnetic dipoles within the *G*-type AFM array resulting in a significant increase in magnetization.

DOI: 10.1103/PhysRevB.81.020103 PACS number(s): 77.84.−s, 63.70.+h, 75.30.Kz

$BiFeO_3$ has attracted considerable attention because of its multiferroic properties that render it a potential candidate for several device applications.[1,2] This compound crystallizes with a perovskite-like structure and, at room temperature, exhibits rhombohedral *R*3*c* symmetry characterized by antiphase $a^-a^-a^-$ octahedral tilting and off-center cation displacements.[3,4] $BiFeO_3$ typically cannot be synthesized as a single phase via solid-state reaction of Bi_2O_3 and Fe_2O_3. Bulk ceramic samples are commonly obtained with traces of one or both of the neighboring equilibrium phases (Bi_2FeO_9 and $Bi_{25}FeO_{40}$).[5–7] On heating, the ferroelectric (FE) rhombohedral phase of $BiFeO_3$ undergoes a first-order phase transition at $T_C \approx 820$ °C to a paraelectric (PE) orthorhombic $GdFeO_3$-type structure.[8] This high-temperature polymorph exhibits $a^+b^-b^-$ octahedral tilting[9] described by *Pbnm* (no. 62, nonstandard setting) symmetry and lattice parameters $\sqrt{2}a_c \times \sqrt{2}a_c \times 2a_c$ ($a_c \approx 4$ Å refers to an ideal cubic perovskite).[8,10] The *R*3*c* $\leftrightarrow$ *Pbnm* transition is somewhat unusual as the symmetry is lower in the high-temperature phase and is accompanied by a large volume change (*expansion* on cooling) of $\approx$1.6%.[8] A similar large volume change has been reported for $Bi_{0.8}La_{0.2}FeO_3$ (Ref. 11) and $BiFe_{0.7}Mn_{0.3}O_{3+\delta}$ (Ref. 12). For comparison, the volume change across the tetragonal-to-cubic phase transition in $PbTiO_3$ is $\approx$0.6%. $BiFeO_3$ also undergoes paramagnetic (PM) to antiferromagnetic (AFM) ordering (on cooling) at $T_N \approx 360$ °C.[13] The AFM arrangement is of the *G* type modified by a long-wavelength ($\approx$620 Å) spiral modulation associated with a canting of magnetic moments.[13] This modulation allegedly inhibits development of a net magnetization in $BiFeO_3$. *A*-site substitutions of rare-earth (RE) cations (La, Sm, Gd, and Nd) in $BiFeO_3$ suppress the spiral magnetic modulation yielding a detectable ferromagnetic response.[14–16]

In the solid solution $Bi_{1-x}Nd_xFeO_3$, an antiferroelectric (AFE) $PbZrO_3$-type orthorhombic phase exists between 300 °C and room temperature for compositions $0.15 \leq x \leq 0.25$.[17] Similar results have also been reported for epitaxial thin films of $(Bi_{0.86}Sm_{0.14})FeO_3$.[18] The $PbZrO_3$ structure (*Pbam*, $\sqrt{2}a_c \times 2\sqrt{2}a_c \times 2a_c$) combines $a^0b^-b^-$ octahedral tilting with antipolar Pb displacements[19] (Fig. 1, denoted as $\mathbf{O_2}$). X-ray powder-diffraction patterns of AFE $(Bi,Nd)FeO_3$ can be fully indexed assuming a $PbZrO_3$-type structure; however, electron diffraction revealed additional superstructure reflections which require a $\sqrt{2}a_c \times 2\sqrt{2}a_c \times 4a_c$ supercell.[17] These extra reflections were attributed to a complex $NaNbO_3$-like $(a^-a^-c^+)/(a^-a^-c^-)$ octahedral tilting[20] but the exact structure of the antipolar $(Bi,Nd)FeO_3$ phase remained uncertain.[17] Tentative phase

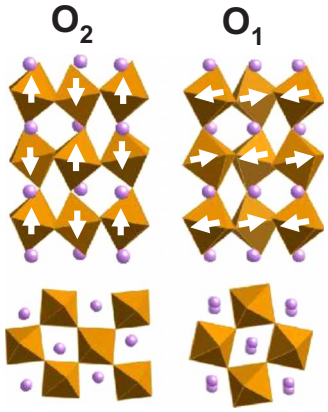

FIG. 1. (Color online) Schematic rendering of the structures for the $\mathbf{O_1}$ and $\mathbf{O_2}$ polymorphs in $Bi_{0.825}Nd_{0.175}FeO_3$ (x=0.175) refined using neutron-diffraction data collected at 25 °C and 350 °C, respectively. Directions of the magnetic moments are indicated using white arrows.

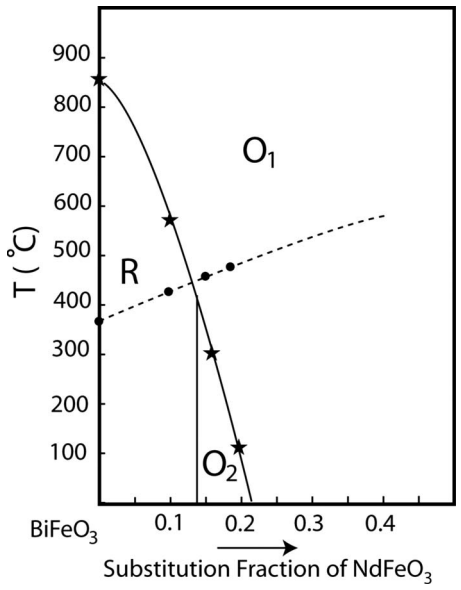

FIG. 2. A T_0 diagram for the Bi-rich part of the $BiFeO_3$-$NdFeO_3$ system. Solid and dashed lines correspond to the structural and magnetic phase transitions, respectively. Experimentally determined transition temperatures (present study) are indicated using symbols. T_0 values for the magnetic transition were inferred from the variable-temperature magnetic measurements. **R** refers to the rhombohedral structure, whereas $\mathbf{O_1}$ and $\mathbf{O_2}$ refer to the $GdFeO_3$- and $PbZrO_3$-type structures, respectively.

diagrams for the (Bi,RE)FeO_3 systems[21] suggested the phase transition sequence $R3c$ (labeled as **R**) $\leftrightarrow Pbnm(\mathbf{O_1})$ and $Pbam(\mathbf{O_2}) \leftrightarrow Pbnm(\mathbf{O_1})$, depending on composition (Fig. 2). In the present study, we combined high-temperature x-ray, neutron, and electron diffraction to further study the transitions in ceramic $Bi_{1-x}Nd_xFeO_3$ ($0 \leq x \leq 0.2$), a detailed account of which will be presented elsewhere. This contribution, however, focuses on the $\mathbf{O_2} \leftrightarrow \mathbf{O_1}$ (AFE $\leftrightarrow$ PE) phase transition and its effect on the magnetic structure and properties.

$Bi_{1-x}Nd_xFeO_3$ samples (x=0.1, 0.15, 0.175, and 0.2) were prepared by conventional solid-state synthesis. Bi_2O_3 (99.999%), Nd_2O_3 (99.999%), and Fe_2O_3 (A.G.) powders were mixed in acetone using an agate mortar and pestle, dried, pressed into pellets and heat treated in air at 850 °C for 5 h. The Nd_2O_3 powder was preheated at 700 °C prior to weighing to remove any residual moisture. The samples were subjected to multiple heat treatments (with intermediate grindings) at 920 °C for a total time of 200 h until no detectable changes in the width of x-ray reflections could be observed. Thermogravimetric analyses indicated no detectable weight loss under these heat-treatment conditions.

X-ray diffraction (XRD) patterns were collected using a Panalytical X'pert Pro diffractometer equipped with a Ge single-crystal incident beam monochromator (Cu $K_{\alpha 1}$ radiation), a Pixcel position sensitive detector, and an Anton Paar HTK-16 high-temperature stage. A Philips CM30 TEM operated at 200 kV and equipped with a double-tilt high-temperature stage was used for electron diffraction and imaging. Neutron powder-diffraction data were collected using the BT-1 [wavelength 1.5402(2) Å] and POLARIS (time-of-flight) instruments located at NIST and ISIS (Rutherford Appleton Laboratory), respectively. In both cases, the sample powders were loaded in vanadium containers. Rietveld refinements were performed using the GSAS software package.[22] The SARAh software[23] was combined with GSAS for symmetry-constrained magnetic-structure refinements. Variable field (from +5570 kA/m=70 000 Oe to −5570 kA/m) and temperature (from 300 to 1000 K) magnetic measurements were performed on sintered pellets using a Quantum Design superconducting quantum interference device vibrating-sample magnetometer equipped with a sample oven that extends the maximum operating temperature to 1000 K. Before each variable-temperature scan, the sample was first subjected to a strong magnetic field of 70 000 Oe, and the field was then reduced to a selected value.

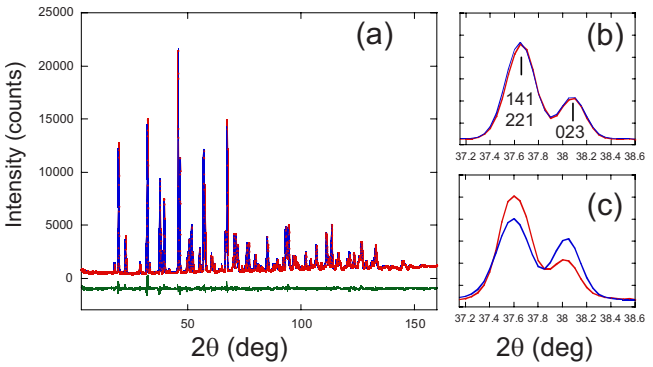

FIG. 3. (Color online) (a) Upper: experimental (red/symbols) and calculated (blue/line) constant-wavelength neutron-diffraction profiles for the $\mathbf{O_2}$ phase of $Bi_{0.825}Nd_{0.175}FeO_3$ (x=0.175) at room temperature. Lower: residual (R_{wp}=4.18%, χ^2=2.44). The calculated profile corresponds to the $PbZrO_3$-like model with *Pbam* symmetry; (b) fit for a pair of reflections (141/221 and 023) for the models with *c*- (b) and *a*-axis (c) orientations of the magnetic moments. Similar results were obtained for x=0.15.

As described previously,[17] room-temperature XRD patterns for x=0.1 are accounted for by the rhombohedral $R3c$ structure, whereas those for $0.15 \leq x \leq 0.2$ can be fitted using a $PbZrO_3$-type *Pbam* structure. The XRD patterns reveal no clear evidence for a doubling of the unit cell from $\sqrt{2}a_c \times 2\sqrt{2}a_c \times 2a_c$ to $\sqrt{2}a_c \times 2\sqrt{2}a_c \times 4a_c$, as suggested by the observation of $\frac{1}{4}[001]_c$-type superlattice reflections in electron diffraction.[17] Likewise, room-temperature neutron powder-diffraction data collected for x=0.15 and x=0.175 are satisfactorily fitted using the $PbZrO_3$-like *Pbam* model which readily accounts for all observed reflections (Fig. 3). Nevertheless, large and highly anisotropic atomic displacement parameters for the oxygen and Bi/Nd positions indicate that the actual structure for these samples deviates slightly from *Pbam* symmetry. Reflection conditions $0kl: k+l=2n$ and $h0l: h=2n$ in electron-diffraction patterns for the samples with $0.15 \leq x \leq 0.2$ (Ref. 17) limit the choice of possible space groups for the $\sqrt{2}a_c \times 2\sqrt{2}a_c \times 4a_c$ superstructure to *Pnam* (no. 62) and $Pna2_1$ (no. 33). *Pnam* symmetry matches a structure with $NaNbO_3$-like octahedral tilting and $PbZrO_3$-like antipolar displacements of the *A* cations; such complex $(a^-a^-c^+)/(a^-a^-c^-)$ tilting appears plausible consid-

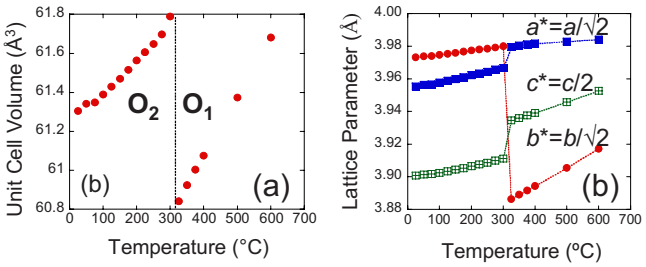

FIG. 4. (Color online) Temperature dependence of the unit-cell volume (a) and lattice parameters (b) for $x=0.15$. The unit-cell volume and lattice parameters were reduced to those of a cubic perovskite cell with $a_c \approx 4$ Å. In Fig. 1, the a axis is parallel to the viewing direction and the b axis is horizontal for both $\mathbf{O_1}$ and $\mathbf{O_2}$.

ering a competition between the $a^-a^-a^-$ and $a^+b^-b^-$ tilts exhibited by the parent phases $BiFeO_3$ and $NdFeO_3$, respectively. Attempts to refine this model using the neutron-diffraction data produced no significant improvement in the fit, though relatively strong correlations among structural variables in the larger model precluded refinements of anisotropic displacement parameters. We conclude that $NaNbO_3$-like tilting is not strong and/or sufficiently ordered to significantly contribute to the powder-diffraction patterns at room temperature.

High-temperature x-ray, electron-, and neutron-diffraction experiments confirmed that all $(Bi,Nd)FeO_3$ samples undergo a phase transition on heating to the $\mathbf{O_1}$ $GdFeO_3$-like structure (Fig. 1) in agreement with the proposed phase diagram (Fig. 2). The transition temperature decreases rapidly from ≈ 600 °C for $x=0.10$ to ≈ 300 °C for $x=0.15$ to ≈ 120 °C for $x=0.20$ (Fig. 2).[24] Despite the same no. 62 space group for both the $\mathbf{O_2}$ and $\mathbf{O_1}$ structures, their symmetries do not obey group-subgroup relations and the $\mathbf{O_2} \leftrightarrow \mathbf{O_1}$ transition is first order. Likewise, the $\mathbf{R} \leftrightarrow \mathbf{O_2}$ transition (Fig. 2), which presumably occurs in a very narrow compositional range, must be first order. A large discontinuous volume change, similar to that encountered in $BiFeO_3$, is observed upon both $\boldsymbol{R} \leftrightarrow \mathbf{O_1}$ and $\mathbf{O_2} \leftrightarrow \mathbf{O_1}$ transitions [Fig. 4(a)], even though the structural changes underlying these two transitions are different. This large volume change at relatively low temperatures explains the fragility of the sintered pellets after cooling to room temperature. Figure 4(b) summarizes changes in the lattice parameters (reduced to a pseudocubic ≈ 4 Å perovskite cell) across the $\mathbf{O_2} \leftrightarrow \mathbf{O_1}$ transition for $x=0.15$. A large volume effect is determined by the changes in the b^* dimension (horizontal in Fig. 1). The exact structural changes/distortions underlying the large change in the b-axis parameter remain to be clarified. Detailed neutron *total* scattering studies aimed at simultaneous analyses of changes in the local and average distortions across the $\mathbf{O_2} \leftrightarrow \mathbf{O_1}$ phase transition are planned and will be reported separately.

Rietveld refinements of the room-temperature magnetic structure for all compositions confirm an overall G-type AFM ordering (Fig. 3) but powder-diffraction data do not support refinements of a spiral modulation, if present. In the $\mathbf{O_2}$ phase, the magnetic moments are aligned with the c axis of the $\sqrt{2}a_c \times 2\sqrt{2}a_c \times 2a_c$ cell (Fig. 1, left) as evidenced by the characteristic intensity distribution for a pair of reflections 141/221 and 023 in the neutron-diffraction patterns (Fig. 3). The refined value of the magnetic moment for Fe^{3+} is $m=3.75(2)\mu_B$. The directions of magnetic moments in the $\mathbf{O_2}$ phase are orthogonal to those in the room-temperature AFM $Pbnm$ structure of $NdFeO_3$. The AFM ordering is preserved upon the $\mathbf{O_2} \leftrightarrow \mathbf{O_1}$ transition but the magnetic moments in the high-temperature $\mathbf{O_1}$ phase become predominantly aligned with the a axis ($\approx \sqrt{2}a_c$) (Fig. 1, right); that is, neutron diffraction suggests a pronounced coupling between the displacive and magnetic ordering manifested in the reorientation of magnetic moments by 90° at the displacive phase transition (Fig. 1). $NdFeO_3$ also undergoes reorientation of magnetic moments (without a structural transition) but in the reverse direction, i.e., from aligned parallel to the a axis at room temperature to the c axis below 190 K.[25]

Magnetic measurements provide further evidence for a significant effect of the displacive transition $\mathbf{O_2} \leftrightarrow \mathbf{O_1}$ on the

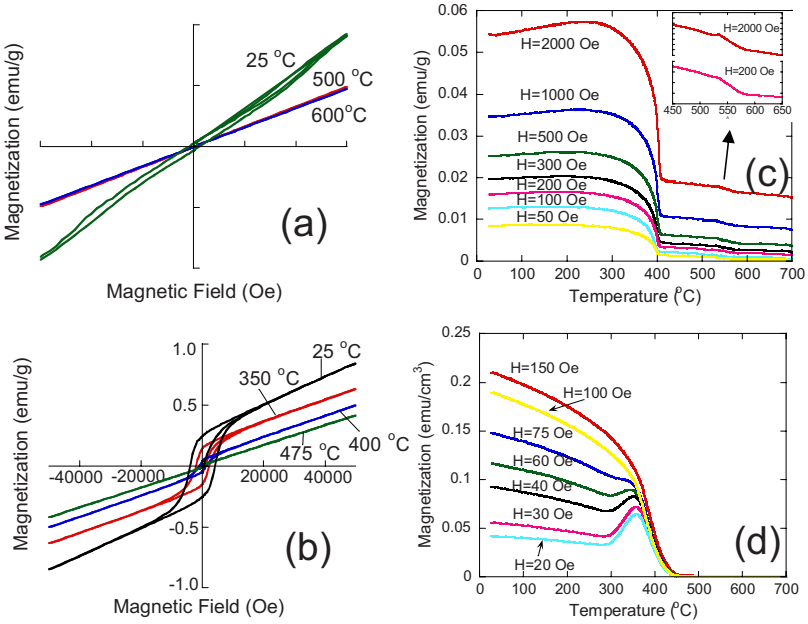

FIG. 5. (Color online) Field (H) dependence of magnetization (M) for the (a) $Bi_{0.9}Nd_{0.1}FeO_3$ and (b) $Bi_{0.85}Nd_{0.15}FeO_3$ samples at selected temperatures. [(c) and (d)] Temperature dependence of magnetization under different external fields for the same samples, respectively. Prior to each variable-temperature scan the samples were first subjected to a magnetic field of 70 000 Oe, and, then, the field was reduced to a selected value.

magnetic response (Fig. 5). At room temperature, the $x=0.1$ sample exhibits only a slim hysteresis loop [Fig. 5(a)], whereas the $x=0.15$ [Fig. 5(b)] and $x=0.20$ (not shown) samples yield robust loops with coercive fields of $H_c \approx 4170$ Oe and $H_c \approx 1950$ Oe, respectively; in all cases, the response changes to paramagnetic at high temperatures. The magnetic phase transition is clearly manifested in a large increase in magnetization [Figs. 5(c) and 5(d)]. The origin of the ferromagnetic response in the Nd-doped $BiFeO_3$ requires further investigation. Importantly, a pronounced peak of magnetization was also observed around the temperatures of the structural phase transition; the temperature of peak magnetization varies somewhat with the applied field. For $x=0.1$, where the structural transition occurs in the PM state, the peak is weak [inset in Fig. 5(c)] and most prominent for larger fields. In contrast, for $x=0.15$ [Fig. 5(d)], this peak becomes pronounced for weak fields because for strong fields the effect is masked by a marked increase in magnetization upon crossing the magnetic transition. The results concur with the reorientation of magnetic dipoles upon the structural transition as suggested by neutron refinements. Conceivably, even in the PM state, the magnetic moments are preferentially aligned with one of the crystallographic axes, and the weak peak of magnetization for $x=0.1$ is caused by reorientation of the moments which is further facilitated by applied magnetic field. For $x=0.2$, where the structural transition occurs well below the temperature of magnetic ordering, the peak of magnetization was evident even at large (e.g., 2000 Oe) fields.

In summary, our results demonstrate that a large volume change encountered during the high-temperature phase transition in $BiFeO_3$ is maintained upon Nd substitution and is particularly evident for the AFE↔PE transition between the $PbZrO_3$-like and $GdFeO_3$-like structures (Fig. 2). Magnetic measurements confirm a robust FM response for the AFE phase and reveal a strong effect of the structural phase transition on magnetization. According to neutron diffraction, the AFE↔PE transition is accompanied by a ≈90° reorientation of the magnetic dipoles in the *G*-type AFM array. More detailed studies of the interplay between the structural and magnetic transitions in this and other rare-earth doped $BiFeO_3$ systems are warranted to understand changes in magnetization with field and temperature.

Experiments at the ISIS Pulsed Neutron and Muon Source were supported by a beam time allocation from the Science and Technology Facility Council. The authors acknowledge Terrell Vanderah (NIST) for her help with the DSC/TGA measurements and Bob McMichael (NIST) for useful discussions.

*Corresponding author.
†igor.levin@nist.gov
‡i.m.reaney@sheffield.ac.uk
§Also at Department of Materials Science and Engineering, University of Maryland, College Park, MD 20742, USA.

[1] G. Catalan and J. F. Scott, Adv. Mater. **21**, 2463 (2009).
[2] R. Ramesh and N. A. Spaldin, Nature Mater. **6**, 21 (2007).
[3] J. M. Moreau, C. Michel, R. Gerson, and W. J. James, J. Phys. Chem. Solids **32**, 1315 (1971).
[4] F. Kubel and H. Schmid, Acta Crystallogr. B **46**, 698 (1990).
[5] R. Palai, R. S. Katiyar, H. Schmid, P. Tissot, S. J. Clark, J. Robertson, S. A. T. Redfern, G. Catalan, and J. F. Scott, Phys. Rev. B **77**, 014110 (2008).
[6] M. Valant, A.-K. Axelsson, and N. Alford, Chem. Mater. **19**, 5431 (2007).
[7] M. W. Lufaso, T. A. Vanderah, I. M. Pazos, I. Levin, R. S. Roth, J. C. Nino, V. Provenzano, and P. K. Schenck, J. Solid State Chem. **179**, 3900 (2006).
[8] D. C. Arnold, K. S. Knight, F. D. Morrison, and P. Lightfoot, Phys. Rev. Lett. **102**, 027602 (2009).
[9] A. M. Glazer, Acta Crystallogr. B **28**, 3384 (1972).
[10] M. Marezio, J. P. Remeika, and P. D. Dernier, Acta Crystallogr. B **26**, 2008 (1970).
[11] M. Polomska, W. Kaczmarek, and Z. Pajak, Phys. Status Solidi **23**, 567 (1974).
[12] S. M. Selbach, Th. Tybell, M.-A. Einarsrud, and T. Grande, Phys. Rev. B **79**, 214113 (2009).
[13] I. Sosnowska, T. Peterlin-Neumaier, and E. Steichele, J. Phys. C **15**, 4835 (1982).
[14] G. L. Yuan, S. W. Or, J. M. Liu, and Z. G. Liu, Appl. Phys. Lett. **89**, 052905 (2006).
[15] V. A. Khomchenko, V. V. Shvartsman, P. Borisov, W. Kleeman, D. A. Kiselev, I. K. Bdikin, J. M. Vieira, and A. L. Kholkin, Acta Mater. **57**, 5137 (2009).
[16] K. S. Nalwa and A. Garg, J. Appl. Phys. **103**, 044101 (2008).
[17] S. Karimi, I. M. Reaney, I. Levin, and I. Sterianou, Appl. Phys. Lett. **94**, 112903 (2009).
[18] C. J. Cheng, D. Kan, S. H. Lim, W. R. McKenzie, P. R. Munroe, L. G. Salamanca-Riba, R. L. Withers, I. Takeuchi, and V. Nagarajan, Phys. Rev. B **80**, 014109 (2009).
[19] E. Sawaguchi, H. Maniwa, and S. Hoshino, Phys. Rev. **83**, 1078 (1951).
[20] A. M. Glazer, M. Ahtee, and H. D. Megaw, Acta Crystallogr. A **28**, S179 (1972).
[21] S. Karimi, I. M. Reaney, Y. Han, J. Pokorny, and I. Sterianou, J. Mater. Sci. **44**, 5102 (2009).
[22] A. C. Larson and R. B. Von Dreele, Los Alamos National Laboratory LAUR Report No. 86-748, 1994 (unpublished).
[23] A. S. Wills, Physica B **276**, 680 (2000).
[24] The transition temperatures reported in this study should be considered as approximate. Accurate determination of these temperatures is limited by the difficulties in achieving a fully homogeneous distribution of Bi and Nd using solid-state synthesis.
[25] J. Bartolomé, E. Palacios, M. D. Kuz'min, F. Bartolome, I. Sosnowska, R. Przenioslo, R. Sonntag, and M. M. Lukina, Phys. Rev. B **55**, 11432 (1997).